energies

MDPI

Article

Addressing Abrupt PV Disturbances, and Mitigating Net Load Profile's Ramp and Peak Demands, Using Distributed Storage Devices

Roshan Sharma* and Masoud Karimi-Ghartemani

Department of Electrical and Computer Engineering, Mississippi State University, Starkville, MS 39762, USA; karimi@ece.msstate.edu

* Correspondence: rs2142@msstate.edu

Received:10 January 2020; Accepted: 21 February 2020; Published: 25 February 2020

Abstract: At high penetration level of photovoltaic (PV) generators, their abrupt disturbances (caused by moving clouds) cause voltage and frequency perturbations and increase system losses. Meanwhile, the daily irradiation profile increases the slope in the net-load profile, for example, California duck curve, which imposes the challenge of quickly bringing on-line conventional generators in the early evening hours. Accordingly, this paper presents an approach to achieve two objectives: (1) address abrupt disturbances caused by PV generators, and (2) shape the net load profile. The approach is based on employing battery energy storage (BES) systems coupled with PV generators and equipped with proper controls. The proposed BES addresses these two issues by realizing flexible power ramp-up and ramp-down rates by the combined PV and BES. This paper presents the principles, modeling and control design aspects of the proposed system. A hybrid dc/ac study system is simulated and the effectiveness of the proposed BES in reducing the impacts of disturbances on both the dc and ac subsystems is verified. It is then shown that the proposed PV-BES modifies the daily load profile to mitigate the required challenge for quickly bringing on-line synchronous generators.

Keywords: PV generator; power ramping; battery energy storage; duck curve; hybrid dc/ac grids

1. Introduction

The limitations of fossil fuel reserves and environmental concerns have increased interest in renewable energy resources [1]. Solar photovoltaic (PV) generation is one of the most promising renewable energy approaches. In recent years, PV power generation has increased significantly thanks to the development of cost-effective, higher efficiency semiconductor PV technology, as well as advancements in related power electronics and controls. Solar PV is projected to contribute 16% of the world's total electricity and 43% of the added electricity in the United States (US) by 2050 [2,3]. However, the uncertainty and variability of PV sources constitute the main obstacles against their high level penetration. Furthermore, PV sources do not have inherent rotational inertia to support the grid during the transients [4–6].

The power injected by PV can change suddenly due to cloud movements. In 2011, a study of three PV systems, located in Porterville, Palmdale, and Fontana, California, found that the power ramp rate was as high as 90%, 93% and 75% per minute of their rated power, respectively [7]. The sudden changes in PV power can introduce voltage fluctuations in distribution system and frequency fluctuations in the case of high PV penetration and weak grid, leading to grid stability issues [2,8–10]. Puerto Rico Electric Power Authority (PREPA) limits the ramp rate to 10%/minute of the rated capacity for both wind and PV generation, and the Hawaiian Electric Company (HECO) limits its ramps at $\pm$2 MW/min

(even ±1 MW/min during some times) for wind generators under 50 MW [11]. According to IEEE standard 1547, distributed energy resources (DERs) cannot cause voltage fluctuations exceeding 3% for a medium voltage interconnection and 5% for a low voltage interconnection [12].

A large number of distributed PV generators together create a duck-shaped daily net load profile due to the variation in solar irradiation. The duck-shaped net load profile has steep slopes, especially in the evening. This requires bringing a large number of synchronous resources online within a short period of time. Such changes in the net load profile cannot be easily addressed by slow conventional generators and the problem becomes severe with the increased penetration of PVs. The existence of a large number of PV generators also increases the chances of negative net load that requires curtailment of PV power [8,13,14].

The number of PV generators connected to the electric power grid has been rising continuously. Authorities and researchers are considering the development of strategies and approaches to obtain grid services, both transient and long-term, from the aggregation of these distributed resources [15]. Therefore, PV generators have been coupled together with complementary generation and storage technologies to address the intermittencies and the disturbances, and these distributed resources are utilized to obtain grid services. Battery energy storage (BES) systems and super-capacitors are two important energy storage approaches that can be coupled with PV generators [16–18].

Most of the existing approaches that combine BES with household PV-prosumers are concerned with optimization of battery size, and energy management strategies to minimize electricity bills [19–21]. These methods do not address the impact of intermittency and power variation of PVs on the grid. Moving average methods are used to mitigate the impact of abrupt PV power disturbances. However, moving average method does not directly control the ramp rate, depends on historical data, and operates the BES even though BES operation is not required due to the memory effect [22]. The direct ramp control of PV power is an effective method. The ramp-up of PV output is generally not a challenging issue, and it can be achieved using a proper controller without requiring a storage, at the expense of total extracted PV energy [23]. However, the ramp-down is a challenge, and it requires an energy storage to compensate for the PV power drop.

The fluctuations of wind/PV generators are compensated using the BES station in Reference [24]. The control approach calculates the target power for the BES station from the fluctuations of wind/PV generators, and this power is shared by the constituting smaller BES units based on their SOC level. In Reference [22], a BES is coupled with a PV system to mitigate the power fluctuations caused by cloud passing using the ramping method. During PV power fluctuations, the BES is controlled based on the inverse characteristics of the desired ramp-rate. Once the PV power fluctuation is over, the BES power is brought to zero using SOC droop-based ramp rate. The control strategies of References [22,24] are presented at system level, and ignore the dynamics of the converter and details of the control design. Furthermore, the BES reference calculations involve complex algorithms. A hybrid BES and super-capacitor setup is used in Reference [25] to provide frequency support. Although this is combined with a PV generator, it does not directly address the PV power generation variations. Moreover, the frequency does not directly and quickly reflect the PV disturbances at the distribution level.

A battery is integrated in an ac-stack architecture in series with PV converters in Reference [26] to achieve the controlled ramp rate in power. The BES control uses the derivative of the rms of ac string current to determine the fluctuation in PV power. This method does not appear to be able to respond to abrupt PV fluctuations in a timely manner due to the limitations with a derivative operator in practice. Furthermore, this architecture is vulnerable to over-modulation that distorts the output. Finally, the stack architecture compromises the plug-and-play flexibility of the system. In Reference [27], a power management strategy is proposed for a BES in connection to a PV and a local load. If the local load is larger than a predefined minimum value, the combined PV-BES supply the load and the rest of power is offset by the grid. No power ramping is done in this mode. If the local load is less than a predefined minimum, the battery performs a ramp rate control, based on Reference [22], if the

PV fluctuations exceed the predefined ramp rate; and the PV-BES operates in constant power feed mode otherwise. Further details of the control design procedures are not presented. A PV-battery combination connected to an ac grid is presented in Reference [28] where the PV operates at the MPP, a battery controls the dc bus voltage of the inverter and the inverter operates in constant power mode. If the reference power of the inverter is properly determined, it can realize ramping. However, this is not discussed in Reference [28]. One limitation of this approach is that the BES cannot be used for an already operating inverter without altering the control system of the inverter. A similar approach is used in Reference [29] where the BES supplies/absorbs the difference of power between the desired and the PV power. The controller in Reference [29] requires communication of an ac signal which is a major limitation. In Reference [30], a 1 MW/2 MWh BES is connected with a multi-MW PV system to achieve (1) power smoothing using moving average and low pass filter, and (2) frequency regulation using P-f droop control. The power smoothing method of Reference [30] has the disadvantages of the moving average approach mentioned earlier. Also, the frequency regulation may not be useful at the distribution level.

Most of the aforementioned works that implement BES to smooth PV power treat the matter at the system level and ignore the dynamics at the converters level. There is a lack of systematic design of the local controls to accomplish the desired power ramps. This paper presents a BES control system concept to address both the abrupt and daily variations of PV power. The proposed BES connects at the terminals of the PV generator (without requiring a change in the PV inverter) and responds to the disturbances to execute desired power ramp rates. The ramp rate signals are either generated locally or received from the grid operator. The paper presents the complete mathematical model of the system including the dynamics of the converter and provides systematic approach in designing the control. Furthermore, if the BES is only used to filter the abrupt PV disturbances for a short period, it results in low utilization of the BES. Therefore, the ramping capability of the PV-BES system has been utilized in this paper to improve the daily load profile. The grid operator can remotely command the distributed PV-BES units with the desired ramp rate, and the proposed control executes the command. The aggregated effect of the distributed PV-BES units with the proposed ramping capability significantly enhances the daily net load profile in terms of (1) reduced peak, (2) increased minimum, and (3) reduced slopes. The proposed method also includes an outer loop that controls the SOC of the BES. The performance of the proposed system is verified using extensive computer simulation and a laboratory prototype.

The contributions of this paper may be summarized as follows: (1) A simple yet effective battery control philosophy to address both the abrupt and daily photovoltaic generation variations. The two set-points of the proposed controller can be generated locally or through communications for system-wide optimization; (2) Complete modeling and control design of the battery control system; (3) Verification of the proposed approach using simulations and laboratory tests.

The remainder of the paper is organized as follows. The power variabilities, abrupt and daily profile, originated from PV generators are discussed in Section 2. Section 3 presents a proposed battery energy storage (BES) system, its mathematical model, and the proposed control to ramp the output power of the PV. Numerical designs and the results obtained both in simulation and laboratory experiment are presented in Section 4. The paper concludes with concluding remarks and limitations of the proposed control in Section 5.

2. Power Variabilities of a PV Generator

2.1. Abrupt Disturbances in PV Generation

Cloud movements cause abrupt changes in solar irradiation, Figure 1. To study the impact of these abrupt power changes, a hybrid dc/ac system is considered in this paper as shown in Figure 2. The parameters of the dc microgrid and the ac system are shown in Tables 1 and 2, respectively. The details of the PV control used in this study are given in Section 4.1.1.

The PV generator of Figure 2 is controlled using a maximum power point tracking (MPPT) algorithm. The control structure and the parameters are shown in Section 4. Figure 3 shows the voltage and frequency fluctuations, at the point of coupling between dc and ac systems, to abrupt PV disturbances. The solar intensity falls from 1000 W/m^2 to 250 W/m^2 at $t = 5.0$ s, and it rises back to 1000 W/m^2 at $t = 50.0$ s. The dc voltage has a peak of 10% that oscillates over a second, and the ac voltage (rms) has a peak close to 5%. The frequency oscillates with a peak of 0.23 Hz, and it takes several seconds to settle.

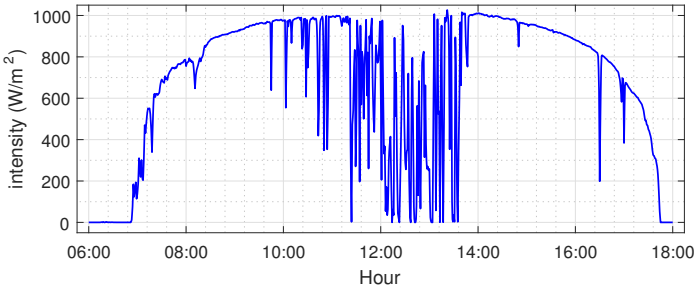

Figure 1. Solar intensity measured at Lowry Range Solar Station on 18 March 2013 [31].

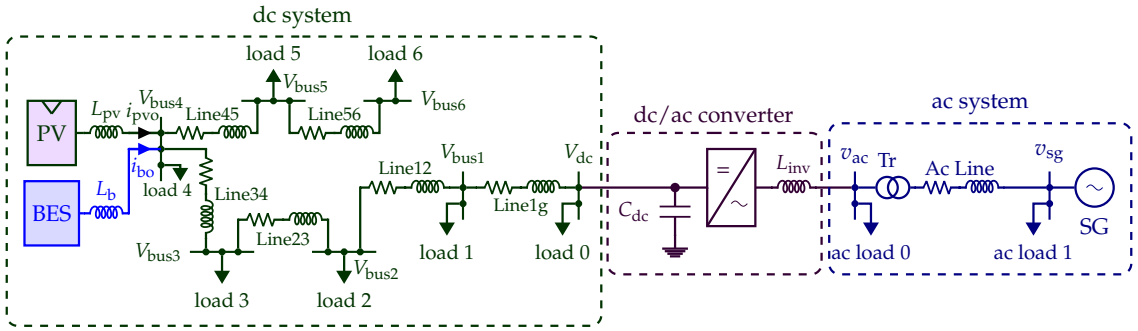

Figure 2. A hybrid dc/ac system to study the abrupt power disturbances of the photovoltaic (PV) generator.

Table 1. Parameters of dc system.

Nominal bus Voltage: 600 V			
Loads:			
Load 0: 1.5 kW	Load 1: 0.5 kW	Load 2: 1.5 kW	
Load 3: 2.0 kW	Load 4: 1.5 kW	Load 5: 5.0 kW	
Load 6: 4.4 kW			
Lines:			
Line	Length	Resistance	Inductance
Line1g	0.75 km	0.482 Ω	0.198 mH
Line12	0.5 km	0.321 Ω	0.132 mH
Line23	0.3 km	0.0.193 Ω	0.079 mH
Line34	0.5 km	0.321 Ω	0.132 mH
Line45	0.5 km	0.321 Ω	0.132 mH
Line56	1 km	0.642 Ω	0.264 mH
PV system:			
Rated power: 15 kW at 1000 W/m^2, 1000 V			

Table 2. Parameters of ac system.

Synchronous Generator (SG):		
Power (S_{sg}): 250 kVA, voltage (v_{sg}): 12.47 V Inertia constant (H): 5.0		
Loads: ac load 0: 0.05 pu, ac load 1: 0.846 pu		
Ac Line: 200 km, 32.2 Ω, 120.96 mH		
Transformer: Resistance (R_{tr}): 0.02 pu, Reactance (X_{tr}): 0.05 pu Voltage ratio (VR): 207.8 V/12.47 kV		
Three-phase dc/ac Converter:		
Parameter	Symbol	Value
Filter inductance	L_{inv}	10 mH
Filter resistance	R_{inv}	10 mΩ
Dc capacitor	C_{dc}	1200 µF
Voltage on dc side	V_{dc}	600 V
Voltage on ac side	V_{ac}	207.8 V

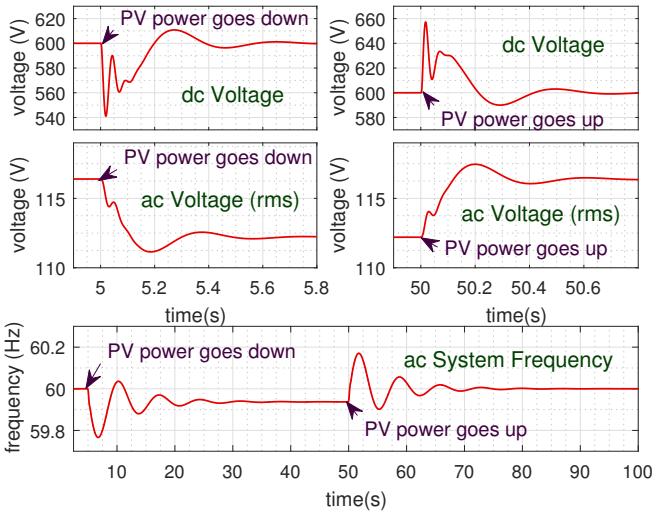

Figure 3. Voltage and frequency fluctuations at point of common coupling (PCC) of the study system due to the abrupt PV disturbances.

2.2. Daily Power Profile of PV

Figure 4a shows the power generation and the load demand of California Independent System Operator (ISO) on 31 March 2019. As the sun rises, the PV generation increases and the net load declines. Into the evening, the PV generation declines while the load demand increases. This creates a duck-shaped net load profile with steep ramp rates. The net profile of Figure 4a has a ramp rate as steep as 5300 MW/h. Such power ramps impose challenges in commitment of the slow conventional generators [32]. The problem becomes severe with the increased penetration level of the PVs as shown in Figure 4b.

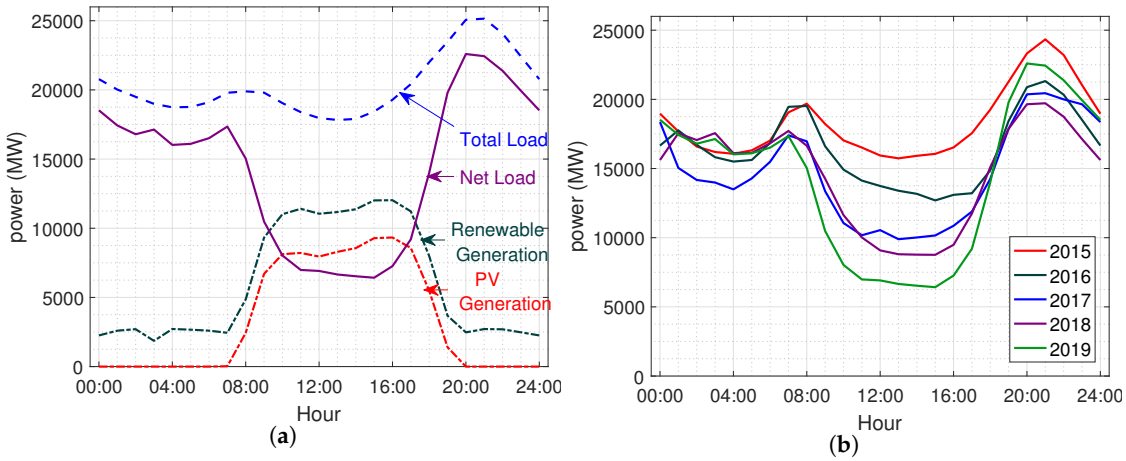

Figure 4. Load profile of California ISO; (**a**) Load demand and generation on 31 March 2019, and (**b**) net load profile on March 31 for last 5 years (2015-19) [33].

3. Proposed BES System and Control

Figure 5 shows the structure of the proposed PV-BES system. The BES connects at the terminals of the PV and executes ramping of the combined power of the PV-BES system. The BES either generates locally or receives the ramp-up-rate (RUR) and ramp-down-rate (RDR) signals from the grid operator and adjusts its operation accordingly. This can (1) prevent the abrupt PV disturbances, and (2) re-shape the daily load profile, as will be demonstrated in this paper.

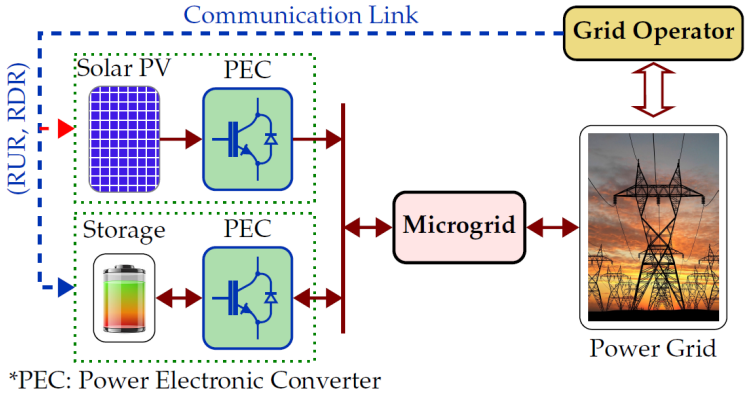

Figure 5. Structure of proposed PV-battery energy storage (BES).

3.1. Defining Operational Scenario of BES

Figure 6a shows the scenario where PV power (P_{pvo}) experiences an abrupt fall followed by an abrupt rise. The BES power, shown in Figure 6b, compensates this sudden disturbance and the combined power of PV-BES system, P_o, has controlled ramp down/up. The charging and discharging of the BES causes rise/fall of its state-of-charge (SOC), as shown in Figure 6c. The BES control system should be equipped with an SOC control that charges/discharges the battery after the response to the disturbance is completed to regulate its SOC to the desired level.

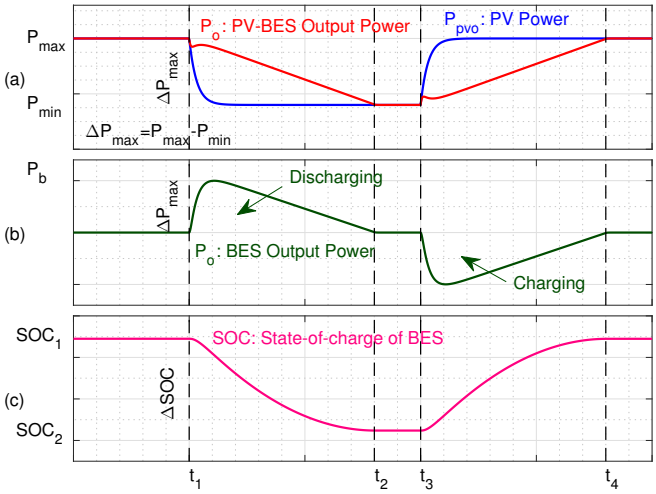

Figure 6. Operational scenario of the BES.

3.2. BES Converter and Its Mathematical Modeling

In this study, the BES uses a bi-directional converter topology as shown in Figure 7. The control system determines the duty cycle of the gating signal for the switches. Assume $d_b(t)$ is the duty cycle of PWM of the BES converter and $v_b(t)$ is the BES voltage, then the average converter voltage is $v_{bo}(t) = d_b(t)v_b(t)$. If $u_b(t) = v_{bo}(t)$ is the control input, then $d_b(t) = \frac{u_b(t)}{v_b(t)}$ and

$$\frac{di_{bo}(t)}{dt} = -\frac{R_b}{L_b} i_{bo}(t) + \frac{1}{L_b} u_b(t) - \frac{V_{bus}}{L_b}, \tag{1}$$

where $i_{bo}(t)$, R_b, L_b, and V_{bus} are the BES converter output current, filter resistance, filter inductance, and the voltage at the point of connection of the BES converter, respectively. In terms of power, (1) can be rewritten as

$$\frac{dP_{bo}(t)}{dt} = -\frac{R_b}{L_b} P_{bo}(t) + \frac{V_{bus}}{L_b} u_b(t) - \frac{V_{bus}^2}{L_b}, \tag{2}$$

where $P_{bo}(t)$ is the output power from the BES system. The dynamics of the SOC depends on the amount of current flowing in/out of the battery and it is mathematically expressed as

$$\frac{d}{dt}\mathrm{SOC}(t) = -\frac{P_{bo}}{Qv_b}, \tag{3}$$

where Q and v_b are the battery capacity (in As) and battery voltage (in V), respectively.

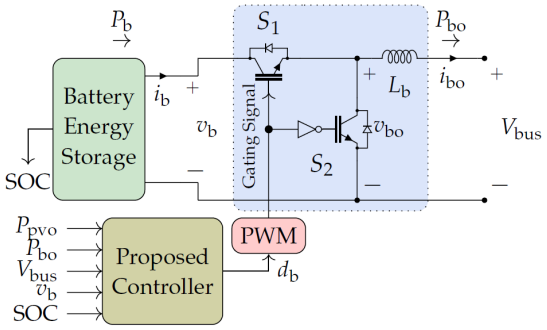

Figure 7. BES converter system.

3.3. BES Control Structure and Design

Figure 8 shows the block diagram of the proposed control structure for the BES system. The control system can be divided into 3 parts: the Power Control (high bandwidth), the Reference Power Calculator, and the SOC control (low bandwidth). These three parts of the controller can be designed separately and independently due to their different time scales.

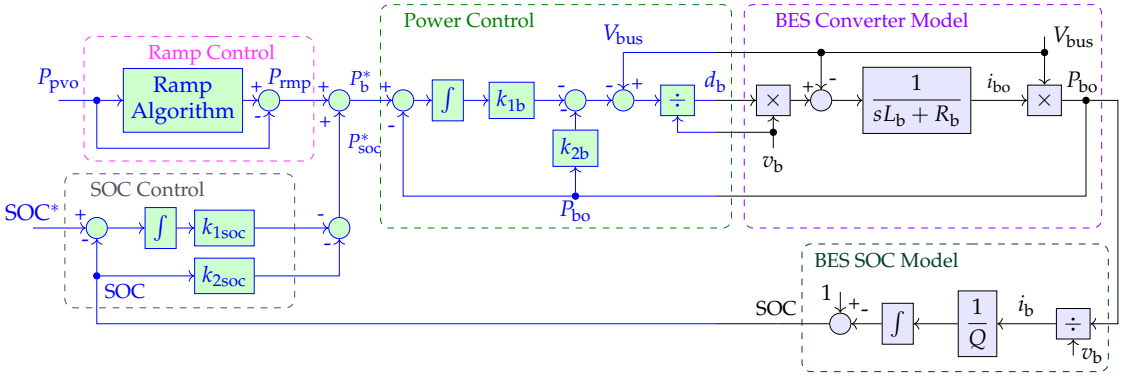

Figure 8. Mathematical model of the BES converter system with the proposed controller.

3.3.1. Power Control Loop

This loop generates the duty cycle for the converter to absorb/supply the reference power (P_b^*). A proportional-integrating (PI) controller is considered and its gains, k_{1b} and k_{2b}, are optimally designed as follows. Define $\dot{x}_1(t) = e(t) = P_b^*(t) - P_{bo}(t)$, and $x_2(t) = P_{bo}(t)$ to obtain the state space equations of the power control loop as

$$\begin{aligned} \dot{x}_1(t) &= -x_2(t) + P_b^*(t) \\ \dot{x}_2(t) &= -\frac{R_b}{L_b} x_2(t) + \frac{V_{bus}}{L_b} u_b(t) - \frac{V_{bus}^2}{L_b}. \end{aligned} \tag{4}$$

We use the approach [34] to convert this tracking problem into standard linear quadratic regulator (LQR) problem by applying $\frac{d}{dt}$ to both sides of (4) to obtain

$$\begin{aligned} \dot{z}_1(t) &= -z_2(t), \\ \dot{z}_2(t) &= -\frac{R_b}{L_b} z_2(t) + \frac{V_{bus}}{L_b} W_b(t), \end{aligned} \tag{5}$$

where $z_i(t) = \dot{x}_i(t)$ and $W_b(t) = \dot{u}_b(t)$. It is assumed that $\frac{d}{dt} V_{bus}$ and $\frac{d}{dt} P_b^*$ are 0, which is justifiable. Therefore, $\dot{z}(t) = Az(t) + BW_b(t)$ and the objective is to regulate $z_1(t) = e(t)$ to 0. The cost function is

$$J = \int_0^\infty [q_1 e^2(t) + q_2 z_2^2(t) + W_b^2(t)] dt. \tag{6}$$

As described in Reference [34], the q_i parameters can be systematically adjusted for the design of the gains (k_{1b}, k_{2b}) to achieve the fast and smooth response in the power control. The numerical design stage for this system is described in Section 4.

3.3.2. Reference Power Calculation

The reference power is calculated using an algorithm to properly follow the desired ramp rate. Figure 9 shows the flowchart that generates a reference power value, P_{rmp}, that follows desired ramp

rate whenever the PV power experiences changes. If P^*_{soc} is power for the SOC control, then the reference power for the BES system is

$$P^*_b(t) = P_{rmp}(t) + P^*_{soc}(t). \tag{7}$$

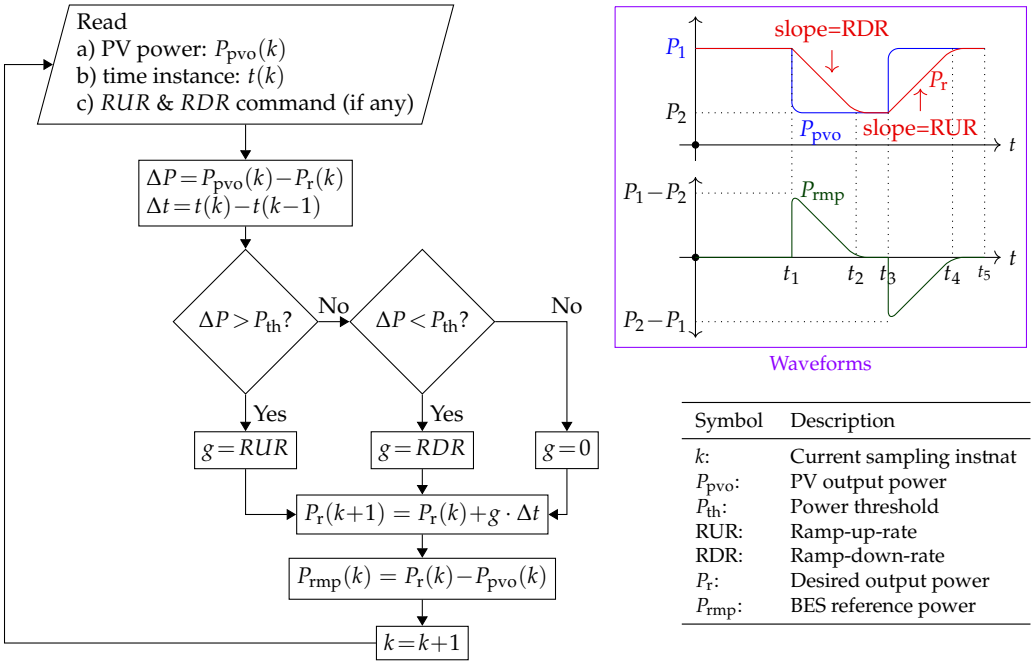

Symbol	Description
k:	Current sampling instnat
P_{pvo}:	PV output power
P_{th}:	Power threshold
RUR:	Ramp-up-rate
RDR:	Ramp-down-rate
P_r:	Desired output power
P_{rmp}:	BES reference power

Figure 9. Flowchart to calculate power ramp reference for the BES.

3.3.3. SOC Control Loop

A PI controller is used and its gains, k_{1soc} and k_{2soc}, are optimally designed to keep the SOC close to its reference value as shown in Figure 8 [6]. The SOC controller gains are designed such that the power control loop and the ramp reference calculator are faster than it. Therefore, during the design of this loop, the fast dynamics of the power control loop may be neglected (and this loop is substituted with a unity gain and the ramp power P_{rmp} is set to zero). With these assumption and also neglecting the small voltage variations across the battery that is, $v_b \approx V^*_b$, the system becomes linear. Defining $\dot{x}_1(t) = e(t) = \text{SOC}^* - \text{SOC}(t)$, $x_2(t) = \text{SOC}(t)$, and $u(t) = P_{soc}(t)$, the state equations of SOC control loop are

$$\begin{aligned} \dot{x}_1(t) &= -x_2(t) + \text{SOC}^*, \\ \dot{x}_2(t) &= -\frac{1}{QV^*_b} u(t). \end{aligned} \tag{8}$$

This can be converted to a LQR form by applying $\frac{d}{dt}$ as

$$\begin{aligned} \dot{z}_1(t) &= -z_2(t), \\ \dot{z}_2(t) &= -\frac{1}{QV^*_b} W_{b1}(t) \end{aligned} \tag{9}$$

where $z_i(t) = \dot{x}_i(t)$. Thus, $\dot{z}(t) = Az(t) + BW_{b1}(t)$ and the objective is to regulate $z_1(t) = e(t)$ to 0. Define the cost function

$$J = \int_0^\infty [q_1 e^2(t) + q_2 z_2^2(t) + W^2_{b1}(t)] dt, \tag{10}$$

and use the method of Reference [34] for the design of the gains (k_{1soc}, k_{2soc}) to achieve smooth response in the SOC control. Numerical design is provided in Section 4.

3.4. Determining the BES Capacity

The battery capacity depends on the desired slowest power ramp of the PV and the BES combined. The minimum BES capacity (Q_{min}) is chosen such that during the maximum power disturbance (ΔP_{max}) the system operates at desired slowest power ramp (R_{min}) keeping the SOC within the desired range (SOC_{min}, SOC_{max}) for all the time.

Figure 6 shows the typical desired response of the system. For maximum PV power fluctuation ΔP_{max} (in W), the BES should be able to supply power with minimum ramp R_{min} (in W/s) for the time interval T where $T = \frac{\Delta P_{max}}{R_{min}}$. Assuming that the battery voltage remains relatively constant at V_b^* (in V) during this period, the total charge supplied by the battery is $\frac{0.5T\Delta P_{max}}{V_b^*}$ (in As). If ΔSOC_{max} is the maximum permissible fluctuation in SOC from its nominal value, SOC_n, during this period, then the minimum battery capacity required, Q_{min} (in As), is given by

$$Q_{min} = \frac{\Delta P_{max}^2}{2V_b^* R_{min} \Delta SOC_{max}}. \quad (11)$$

4. Numerical Designs, Results, and Comparisons

This section presents some numerical designs of the proposed system and also investigates its performance in the context of both abrupt PV power variations and daily irradiation profile using simulations and laboratory-scale experimentation. The structure of the this section is as follows. (1) Section 4.1 studies the performance of proposed system in response to abrupt PV disturbances in a simulated hybrid dc/ac system. (2) Section 4.2 shows the simulation results of applying the proposed system to address abrupt PV disturbances in a real irradiation profile data. (3) Section 4.3 investigates the performance of the proposed method in mitigating the duck-curve phenomenon using simulations on practical data. (4) Section 4.4 shows the results of a laboratory-scale realization of the proposed method. (5) Section 4.5 shows the qualitative comparison of the proposed method with existing methods to mitigate PV power fluctuations.

4.1. Abrupt Disturbances: Case Study 1

The proposed controller is applied to the study system of Figure 2 to study the impact of abrupt PV disturbances. The design of system components are discussed first.

4.1.1. System and Control Parameters

Figure 10 and Table 3 show the PV system and its converter parameters. The controller gains of the PV system are designed using the method discussed in Reference [34]. The internal current loop is designed first, which gives k_{1pv} and k_{2pv}, and then the external loop is designed that includes the design of k_{3pv}, k_{4pv},k_{5pv}, and k_{6pv}. In the design of the external loop, all the dynamics of the internal loop are carried along. Therefore, unlike common practice, the internal loop is not limited to be several times faster than the external loop. In our study, the PV operates at MPPT using perturb and observe (P&O) algorithm [35]. However, this is not a requirement for the proposed BES controller.

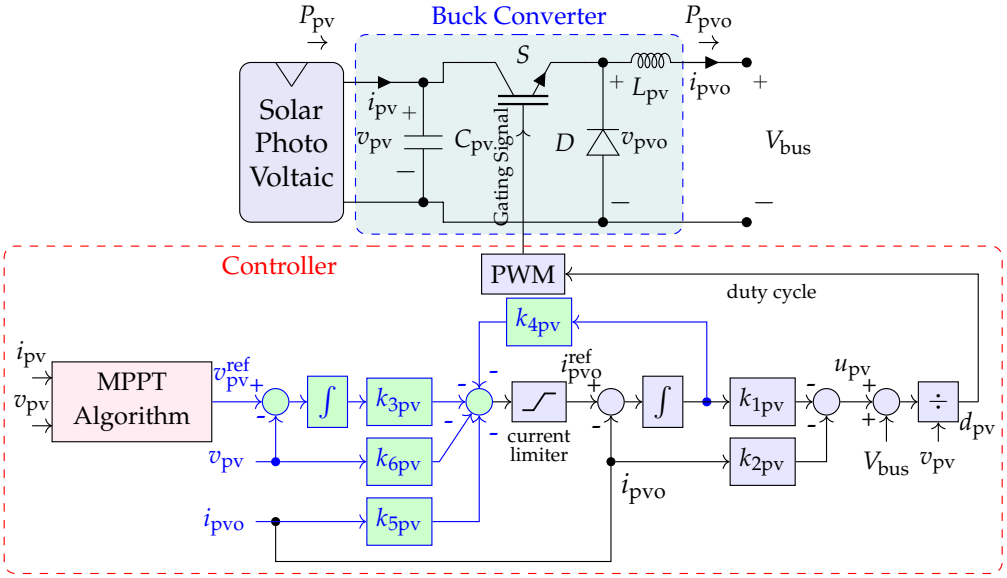

Figure 10. PV converter system and its control.

Table 3. Parameters of PV system.

PV System:
15 kW @ 1000 W/m^2 and 1000 V
V_{bus}: 600 V
Converter:
C_{pv} : 400 µF, L_{pv} : 10 mH, R_{pv}: 10 mΩ
Controller:
Switching Frequency: 10 kHz
Control Gains:
k_{1pv}: −316.22, k_{2pv}: 3.07, k_{3pv}: 31.62
k_{4pv}: 344.49, k_{5pv}: 1.38, k_{6pv}: −0.59

The objective is to obtain the desired ramp rate of 30 %/minute ≈ 75 W/s from the combined PV-BES system. Table 4 shows the parameters of the BES system and its converter. The gains of the power control loop of the BES controller are designed based on the method discussed in Section 3.3.1. Figure 11a shows the plot of the closed loop poles of the power loop on changing q_i's. Here, q_1 and q_2 are subsequently increased between $10^{-3} \rightarrow 10^{2.5}$ and $10^{-6} \rightarrow 10^{-4}$, respectively. The reference power of the BES for the ramp control is calculated by using the method mentioned in Section 3.3.2. For the SOC control loop, the control gains are designed based on the method presented in Section 3.3.3. Figure 11b shows the plot of the closed loop poles of the SOC loop on changing q_i's. Here, q_1 and q_2 are increased between $10^{-1.5} \rightarrow 10^{2.5}$ and $10^{0} \rightarrow 10^{7.75}$, respectively. Table 4 shows the controller gains and the location of the poles for both the power control loop and the SOC control loop. The poles of the SOC control loop are selected such that its speed is several times slower than the ramp rate calculator.

The system and control parameters of the dc/ac converter are adopted based on the conventional voltage source converter (VSC) and vector control method [36–38] to regulate the dc voltage at 600 V. This ensures exchange of power between the dc and ac system in a desired way. The synchronous generator is simulated using the method proposed in Reference [39].

Table 4. BES system parameters.

BES System: V_b: 1000 V, RUR/RDR: 30%/minute ≈75 W/s V_{bus}: 600 V, ΔP_{max}: 15 kW, ΔSOC_{max}: 30% Q_{min}: 5040 As, Choose Q: 5400 As
Converter: L_b:10 mH, R_b:10 mΩ
Controller: Switching Frequency: 10 kHz
Power Control: With q_1: 316.22, q_2: 0.0001 Poles: $-789.6 \pm j665.9$ Gains: k_{1b}: -17.78, k_{2b}: 0.0263
SOC Control: With q_1: 316.22, q_2: 5.62×10^7 Poles $-0.0015 \pm j0.0011$ Gains: k_{1soc}: 17.7828, k_{2soc}: −15,757

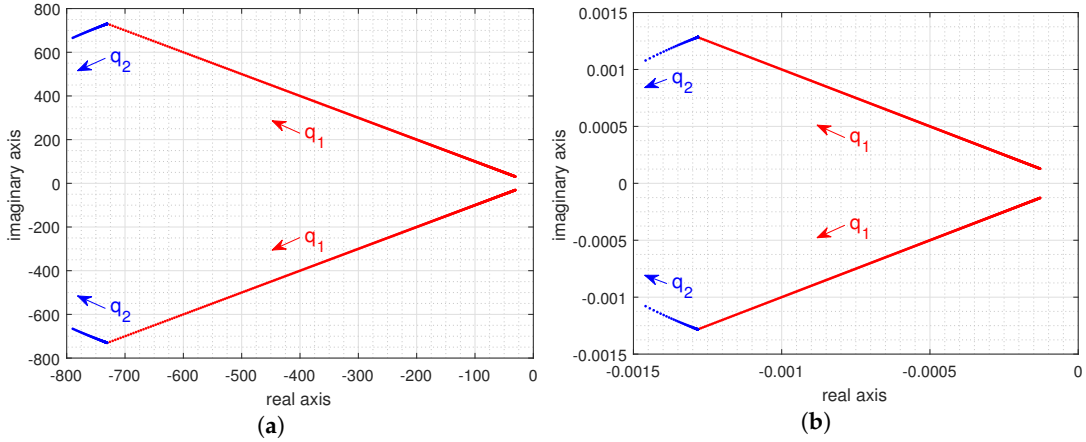

Figure 11. Poles of (**a**) the power, and (**b**) the state-of-charge (SOC) loops of BES.

4.1.2. Results and Discussion

The simulation scenario to study the impact of abrupt PV disturbances is defined as follows. The solar intensity is initially at 1000 W/m^2 and the system is operating at steady state. The PV system supplies 14.2 kW power and there is 1.4 kW power from the ac to the dc system. At $t = 5.0$ s, the solar intensity drops from 1000 W/m^2 to 250 W/m^2 in a fraction of a second that drops the PV power to 3.42 kW. At $t = 50$ s, the solar intensity goes back abruptly to 1000 W/m^2.

Figure 12 shows the output power response of the system. There is a sudden change in the power injected to the dc system (and then flowing into the ac system) when BES is not used. The BES smoothes down those changes and establishes an output power ramp at the desired rate. Figure 13 shows the transient response details of the PV, the BES, and the combined output powers. It confirms that the BES quickly compensates for the PV power practically without a delay.

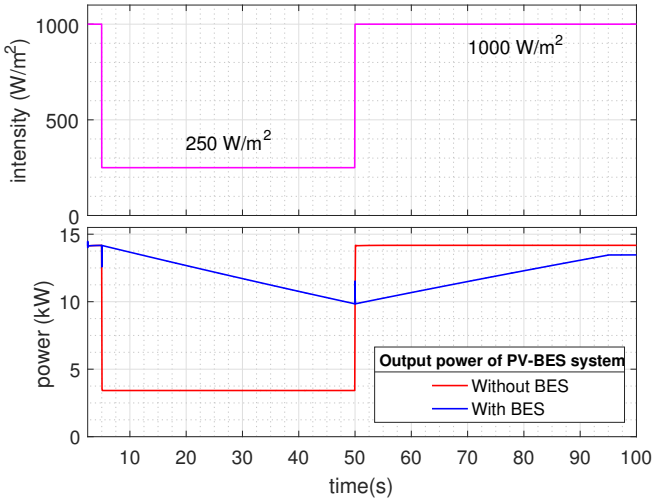

Figure 12. Top: solar irradiance, Bottom: powers of the PV and BES system response to the solar irradiance.

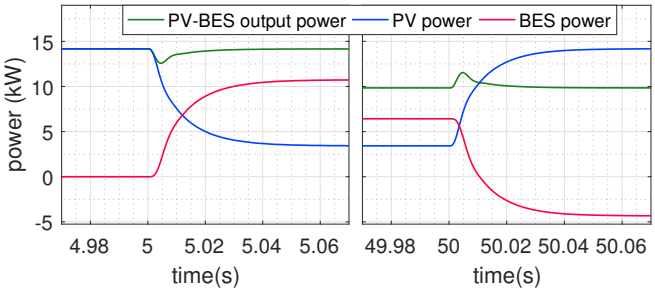

Figure 13. Power transients of the PV-BES system to PV disturbances.

Figure 14 shows the voltage and frequency transients at point of common coupling (PCC) of the dc and the ac system in response to the abrupt PV disturbances. The BES has reduced the peak and duration of both dc and ac voltage transients. The ac voltage (rms) experiences a peak fluctuation of close to 5.5 V (close to 5%) without the BES, and the BES limits the fluctuations within 0.1 V (practically zero). The BES has also improved the transients in the system frequency. Figure 15 shows the voltage transients at different buses in the dc system. The BES reduces the voltage transients across the entire dc system. Without the BES, this disturbances causes voltage fluctuations with peaks of over 10%. The BES reduces the peak of the transients to about 1%, and damps out the oscillations quickly. Over ten times improvement is achieved.

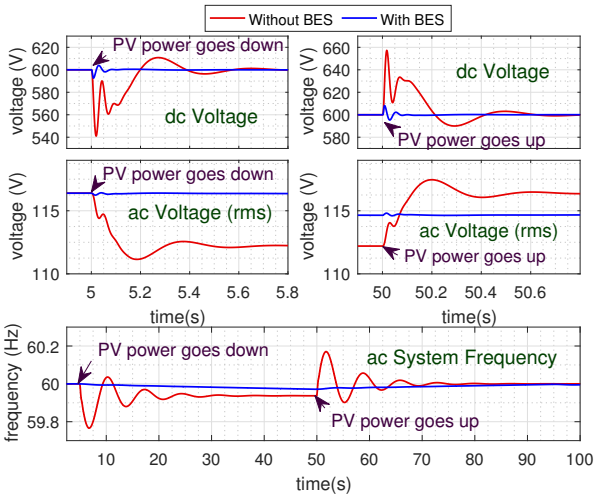

Figure 14. Voltage and frequency due to the abrupt PV disturbances.

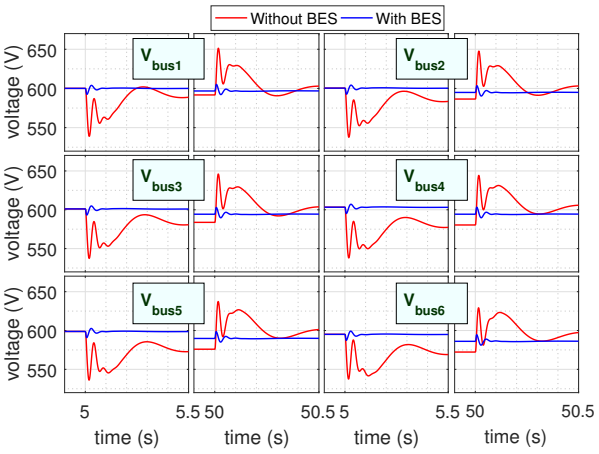

Figure 15. Dc system voltages due to the abrupt PV disturbances.

The ac current of the grid dc/ac converter is shown in Figure 16. When the PV power drops, the ac system supplies the deficit power to the dc system in the absence of the BES. With the proposed BES, the ac current has smooth transitions. Figure 17 shows the SOC of the BES in response to the abrupt PV disturbances. The SOC controller slowly regulates the SOC to the reference value after the disturbance is taken care without affecting the ramping behavior of the BES.

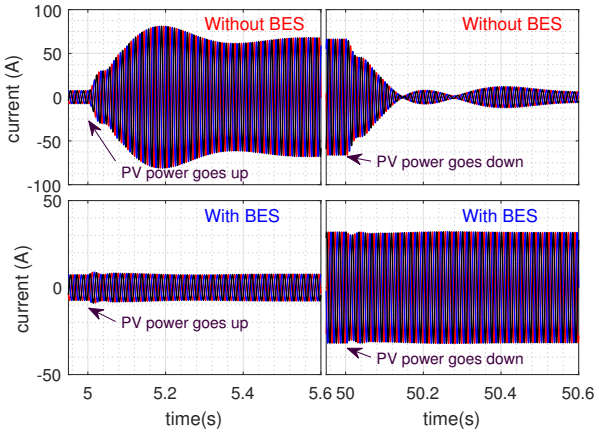

Figure 16. Inverter's ac current due to the abrupt PV disturbances.

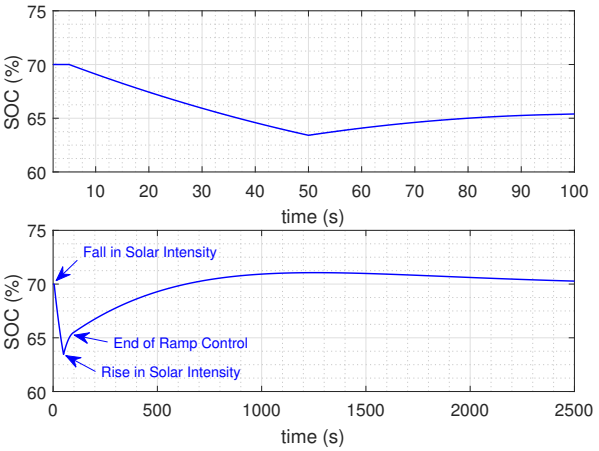

Figure 17. SOC of the BES during and after the abrupt PV disturbances.

4.2. Abrupt Disturbances: Case Study 2

Figure 18 shows the total power of the proposed PV-BES system (designed in previous section) in response to the real solar intensity measured at Lowry Range Solar Station on 18 March 2013 [31] for different power ramp settings (0.5%/minute, 1%/minute, 5%/minute). It demonstrates that the BES reduces the impact of the abrupt PV disturbances and smooths the power profile with the desired ramp rate.

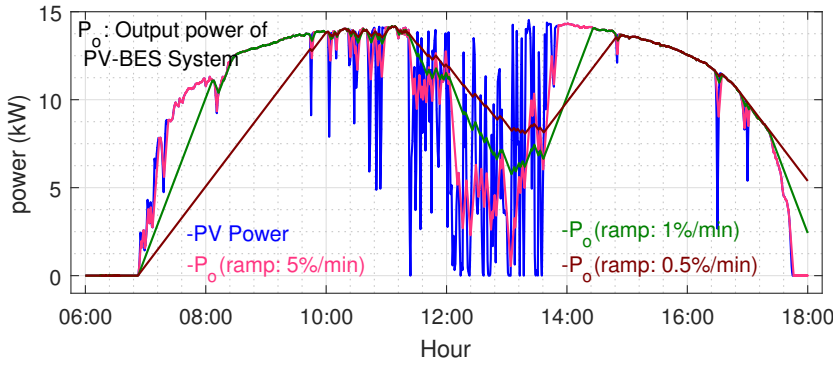

Figure 18. Output power of the proposed PV-BES system for different ramp settings in response to the real solar irradiance data.

4.3. Daily Power Profile of PV

The ramping capability of the proposed PV-BES system can be utilized to shape the daily load profile. When the distributed PV generators are equipped with the proposed BES system, and properly commanded, the aggregated load profile can become much smoother with some desired ramp rates. This also enables peak-load reduction. To demonstrate these properties, two scenarios are studied in this section as follows.

Scenario I: Figure 19 shows the power profile of California ISO on 31 March 2019 [33] with the proposed PV-BES system. The BES charges and stores energy in the morning as the solar intensity increases and avoids sharp decline of net load. This stored energy is released in the evening when the PV generation declines and the load demand increases. Figure 19 shows the profile when both RUR and RDR of the PV-BES system are set at 1200 MW/h. With a total of 5000 MW, 19411 MWh BES systems, the ramp rate is reduced from 5300 MW/h to 2767 MW/h (almost 50%) and the peak load is reduced from 22580 MW to 18747 MW.

Scenario II: In Figure 20, the RUR is set at 1400 MW/h while the RDR is set at 1000 MW/h till 20:00 and changed to 3000 MW/h afterwards. The required BES is 5571 MW, 15201 MWh and the ramp rate of the net load is reduced to 2660 MW/h with peak load of 21535 MW.

The results are summarized in Table 5. This study concludes that by properly adjusting the RUR and RDR, both the steep ramp-up rate and the peak of the net load profile may be mitigated. The RUR and RDR may be optimally computed and supplied by a secondary controller through a low-bandwidth communication.

Table 5. Impact of ramp rate settings on daily power profile.

S.N	Ramp Setting	BES Size		Maximum Ramp in Net Load	Peak Net Load
		Power	Energy		
1	No BES	-	-	5300	22,580
2	RUR: 1200 MW/h RDR: 1200 MW/h	5000 MW	19,411 MWh	2767 MW/h	18,747 MW
3	RUR: 1400 MW/h RDR: 1000 MW/h till 20:00 RDR: 3000 MW/h after 20:00	5571 MW	15,201 MWh	2660 MW/h	21,535 MW

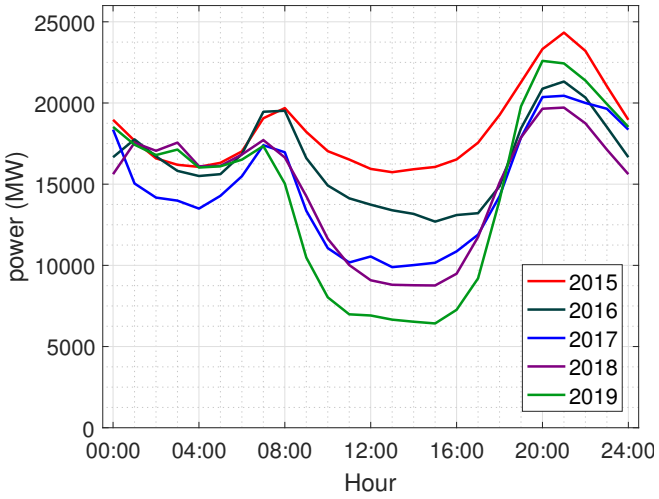

Figure 19. Shaping of Daily Load Profile: Scenario I.

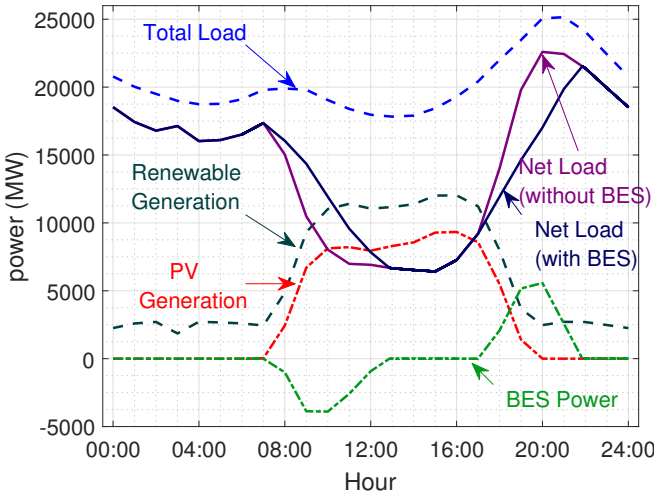

Figure 20. Shaping of Daily Load Profile: Scenario II.

4.4. Experimental Results

This section presents the results of a laboratory-scale implementation of the proposed system to evaluate its performance in a basic condition where all algorithms and controls are implemented in real time. The ability of the proposed approach to counter the PV disturbances (generated using an actual PV emulator hardware and other periphery circuits) is demonstrated. The results confirm feasibility of the proposed algorithms and controls. The details are presented throughout the section.

4.4.1. Experimental Setup

Figure 21 shows a low-power laboratory-scale experimental setup built to evaluate the performance of the proposed controller in response to the abrupt PV disturbances. An Agilent E4360A modular solar array simulator is used to emulate the PV and its disturbances. It is connected to a dc grid via a standard buck converter. A dc power supply in parallel with a local load models the dc grid. Another dc supply with a local load acts as a battery, and it is connected to the dc grid via a half-bridge converter for bi-directional power flow. The proposed control method is used and realized on the micro-controller to control the two converters.

Table 6 shows the system and control parameters. The control parameters for the PV system are designed to regulate the PV voltage to 20 V (maximum power point) using the method discussed in Section 4.1.1. For the BES system, the reference power calculation and the design of the power control

parameters are done using the method in Section 3.3. We have ignored the SOC control and the ac system due to limitations in experimental setup.

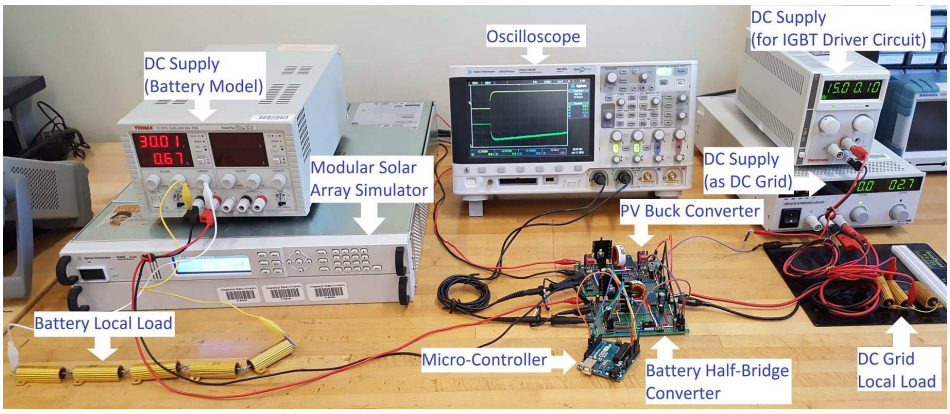

Figure 21. Experimental setup.

Table 6. Experimental setup parameters.

Modular Solar Array Simulator: **PV Curve I**: V_{mp}: 20.0 V, I_{mp}: 0.3 A, V_{oc}: 23.0 V, I_{sc}: 0.5 A **PV Curve II**: V_{mp}: 20.0 V, I_{mp}: 2.0 A, V_{oc}: 23.0 V, I_{sc}: 2.5 A
PV converter: L_{pv}: 1 mH, R_{pv}: 0.2587 Ω, C_{pv}: 100µF
BES and converter: V_b: 30.0 V, Local Load: 30 Ω, L_b: 1 mH, R_b: 0.250 Ω
Dc bus: V_{bus}: 10.0 V, Local Load: 2 Ω
Controller: Switching Frequency: 32 kHz PV converter control gains k_{1pv}: −56.23, k_{2pv}: 0.18, k_{3pv}: 10.00, k_{4pv}: 382.76, k_{5pv}: 1.02, k_{6pv}: −0.16 BES controller settings RUR & RDR: 1.0 W/s, Control Gains: k_{1b}= −5.6234, k_{2b}= 0.0189 (Power control)

4.4.2. Results

Figure 22a shows the response of the system for the ramp rate setting of 1.0 W/s (for both RDR & RUR). Abrupt PV disturbances are manually applied to the PV emulator by switching from PV Curve I to PV Curve II and vice versa as specified in Table 6. When the PV conveter output increases, the battery quickly intervenes to absorb the power. Similarly, the battery supplies power when there is abrupt fall in PV converter power. With the grid voltage of 10 V, the ramp rate of 0.1 A/s in current is obtained. Figure 23 shows the results when the PV power experiences random abrupt disturbances. The study presented in this section confirms that the proposed control system can be successfully implemented in real-time on a typical hardware platform and the desired ramping rates set by the user are achieved by the combination of PV and proposed BES control system.

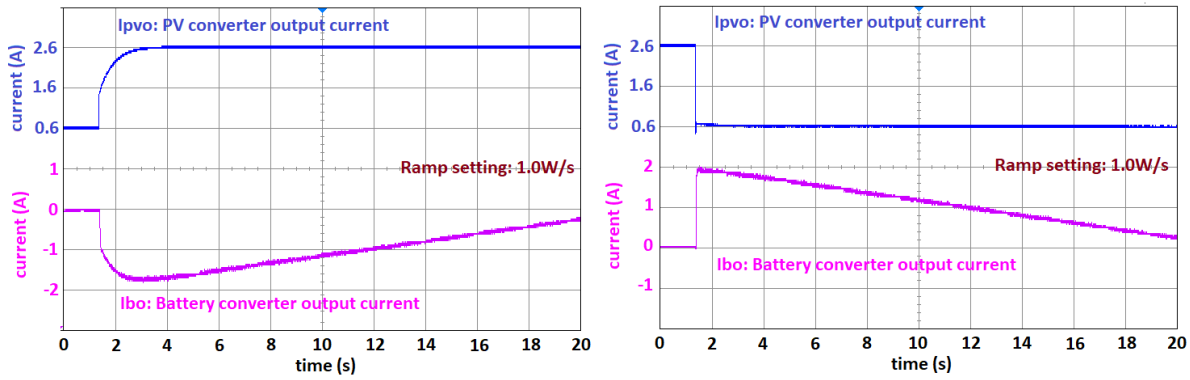

Figure 22. Experimental results: (**a**) ramp up response, and (**b**) ramp down response.

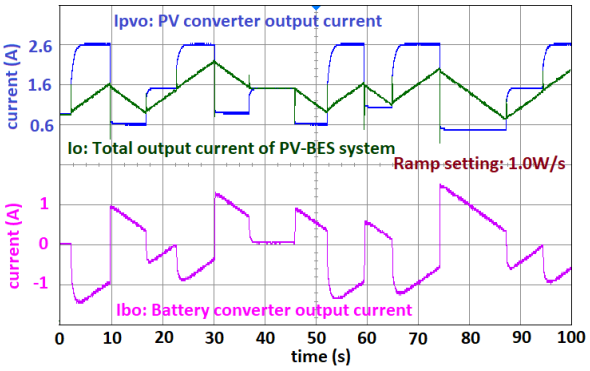

Figure 23. Experimental result: ramp up/down response for random PV power changes.

4.5. Comparisons

This section demonstrates comparison of the proposed method with conventional methods to execute smoothing of PV power. The comparison is done based on various qualitative parameters such as ramp calculation simplicity, plug-play level of proposed BES, coverage of converter model details, optimal control design, and inclusion of SOC control. The evaluation are done at the levels of poor, fair, average, and good. The comparisons are tabulated in Table 7.

Table 7. Qualitative comparison of proposed method with existing methods.

References	Smoothing Method	Ramp Calculation Simplicity	Plug-and-Play Level	Model Details	SOC Control Design	Optimal Control Design
[24]	Ramp	Average	Poor	Fair	No	No
[22]	Ramp	Fair	Poor	Fair	No	No
[25]	P-f droop	Average	Fair	Average	No	No
[26]	Ramp	Fair	Poor	Average	No	No
[27]	Ramp, Constant power	Fair	Fair	Average	No	No
[28]	Constant power	Average	Fair	Average	No	No
[29]	Constant power	Average	Poor	Average	No	No
[30]	Moving average, P-f droop	Fair	Poor	Poor	No	No
Proposed method	Ramp	Good	Good	Good	Yes	Yes

5. Conclusions

PV power experiences abrupt changes due to the fast moving clouds which cause voltage and frequency fluctuations in the weak grid and high PV penetrations. A battery energy storage (BES) is proposed in this paper to address fast power disturbances. Furthermore, the daily profile of the solar irradiance creates sharp ramp in daily load profile, which imposes challenges on the slow conventional generators. The ramping capability of the proposed PV-BES system is utilized to smooth and improve the daily load profile in terms of its steep ramp up and peak demand. Although the concept is developed for a BES system, it can be applied to other behind-the-meter distributed assets such as

small gas turbine generators. The optimal computation and communication of the storage ramp rates are the future directions of research. To mention a limitation, the proposed approach of this paper requires the BES to be co-located with the PV and have access to its terminals in order to achieve the desired power ramping of the combined PV-BES.

Author Contributions: Conceptualization, R.S. and M.K.-G.; Modeling and simulation, R.S.; Formal analysis, R.S. and M.K.-G.; Investigation, R.S.; Writing–original draft preparation, R.S. and M.K.-G.; Writing–review and editing, R.S. and M.K.-G.; Supervision, M.K.-G.; Funding acquisition, M.K.-G. All authors have read and agreed to the published version of the manuscript.

Funding: This research work was partially supported by National Science Foundation (NSF 1808368).

Conflicts of Interest: The authors declare no conflict of interest.

Abbreviations

PV	Photovoltaic	BES	Battery Energy Storage
DER	Distributed Energy Resources	LQR	Linear quadratic regulator
MPPT	Maximum power point tracking	PCC	Point of common coupling
PI	Proportional Integrator	pu	per unit
RDR	Ramp Down Rate	RUR	Ramp Up Rate
SG	Synchronous generator	SOC	State of Charge
ISO	Independent System Operator		

Symbols and Variables

t	Time	k	Sampling instant
Δt	Change in time	S_{sg}	Synchronous generator power
v_{sg}	Voltage of synchronous generator	H	Inertia constant
R_{tr}	Resistance of transformer	X_{tr}	Reactance of transformer
VR	Transformer voltage ratio	V_{dc}	Dc voltage at the PCC
V_{ac}	L-L rms ac voltage at PCC	L_{inv}	Filter inductance of dc/ac converter
R_{inv}	Filter resistance of dc/ac converter	C_{dc}	Capacitor on dc side of dc/ac converter
V_{bus}	Voltage at PV-BES connection	$V_{\mathrm{bus\ i}}$	Voltage of i^{th} bus
RUR	Ramp up rate	RDR	Ramp down rate
R_{min}	Minimum ramp rate	P_{pv}	PV power
P_{pvo}	Output power of PV converter	ΔP	Change in PV power
P_{r}	Desired output power	ΔP_{max}	Maximum change in PV power
P_{o}	Total output power of PV-BES system	L_{pv}	Filter inductance of PV converter
C_{pv}	Capacitor across PV terminals	R_{pv}	Filter resistance of PV converter
$k_{\mathrm{i\ pv}}$	PV control i^{th} gain	i_{pv}	PV current
i_{pvo}	Output current of PV converter	v_{pv}	PV voltage
$v_{\mathrm{pv}}^{\mathrm{ref}}$	PV reference voltage	V_{mp}	PV voltage at maximum PV power
I_{mp}	PV current at maximum PV power	V_{oc}	Open-circuit voltage of PV
I_{sc}	Short-circuit current of PV	P_{b}^{*}	BES reference power
P_{soc}^{*}	Reference power for SOC control of BES	P_{b}	Battery Power
P_{bo}	Output power of BES converter	i_{b}	Battery current
i_{bo}	Output current of BES converter	d_{b}	Duty cycle for BES converter
u_{b}	Control input of BES converter	v_{b}	Battery voltage
V_{b}^{*}	Nominal voltage of battery	SOC	State of charge of BES
SOC_{n}	Nominal SOC of BES	ΔSOC	Change in SOC of BES
$\Delta SOC_{\mathrm{max}}$	Maximum change in SOC	L_{b}	Filter inductance of BES converter
R_{b}	Filter resistance of BES converter	Q	Battery capacity
Q_{min}	Minimum battery capacity	$k_{\mathrm{i\ b}}$	BES power control i^{th} gain
$k_{i\ soc}$	i^{th} gain of SOC control	J	Cost function
q_{i}	i^{th} weighting factor in cost function		

References

1. Al-Hallaj, S. More than enviro-friendly: Renewable energy is also good for the bottom line. *IEEE Power Energy Mag.* **2004**, *2*, 16–22. [CrossRef]
2. Hu, J.; Li, Z.; Zhu, J.; Guerrero, J.M. Voltage Stabilization: A Critical Step Toward High Photovoltaic Penetration. *IEEE Ind. Electron. Mag.* **2019**, *13*, 17–30. [CrossRef]
3. Administration, U.E.I. Annual Energy Outlook 2019: With Projections to 2050. 2019. Available online: https://www.eia.gov/outlooks/aeo/pdf/aeo2019.pdf (accessed on 8 April 2019).
4. Kroposki, B.; Johnson, B.; Zhang, Y.; Gevorgian, V.; Denholm, P.; Hodge, B.M.; Hannegan, B. Achieving a 100% renewable grid: Operating electric power systems with extremely high levels of variable renewable energy. *IEEE Power Energy Mag.* **2017**, *15*, 61–73. [CrossRef]
5. Silwal, S.; Karimi-Ghartemani, M. On Transient Responses of a Class of PV Inverters. *IEEE Trans. Sustain. Energy* **2019**, *10*, 311–314. [CrossRef]
6. Qunais, T.; Sharma, R.; Karimi-Ghartemani, M.; Silwal, S.; Khajehoddin, S.A. Application of Battery Storage System to Improve Transient Responses in a Distribution Grid. In Proceedings of the 2019 IEEE 28th International Symposium on Industrial Electronics (ISIE), Vancouver, BC, Canada, 12–14 June 2019; pp. 52–57.
7. Mather, B.A.; Shah, S.; Norris, B.L.; Dise, J.H.; Yu, L.; Paradis, D.; Katiraei, F.; Seguin, R.; Costyk, D.; Woyak, J.; et al. *NREL/SCE High Penetration PV Integration Project: FY13 Annual Report*; Technical Report; National Renewable Energy Lab. (NREL): Golden, CO, USA, 2014.
8. Katiraei, F.; Aguero, J.R. Solar PV integration challenges. *IEEE Power Energy Mag.* **2011**, *9*, 62–71. [CrossRef]
9. Bueno, P.G.; Hernández, J.C.; Ruiz-Rodriguez, F.J. Stability assessment for transmission systems with large utility-scale photovoltaic units. *IET Renew. Power Gener.* **2016**, *10*, 584–597. [CrossRef]
10. Sakamuri, J.N.; Das, K.; Altin, M.; Cutululis, N.A.; Hansen, A.D.; Tielens, P.; Van Hertem, D. Improved frequency control from wind power plants considering wind speed variation. In Proceedings of the 2016 Power Systems Computation Conference (PSCC), Genoa, Italy, 20–24 June 2016; pp. 1–7.
11. Gevorgian, V.; Booth, S. *Review of PREPA Technical Requirements for Interconnecting Wind and Solar Generation*; Technical Report; National Renewable Energy Lab. (NREL): Golden, CO, USA, 2013.
12. IEEE Std 1547-2018 Standard for Interconnection and Interoperability of Distributed Energy Resources with Associated Electric Power Systems Interfaces. 2018; pp. 1–138. Available online: https://ieeexplore.ieee.org/abstract/document/8332112 (accessed on 8 April 2019).
13. Denholm, P.; O'Connell, M.; Brinkman, G.; Jorgenson, J. *Overgeneration from Solar Energy in California. A Field Guide to the Duck Chart*; Technical Report; National Renewable Energy Lab. (NREL): Golden, CO, USA, 2015.
14. Ghosh, S.; Rahman, S.; Pipattanasomporn, M. Distribution voltage regulation through active power curtailment with PV inverters and solar generation forecasts. *IEEE Trans. Sustain. Energy* **2016**, *8*, 13–22. [CrossRef]
15. Xue, Y.; Guerrero, J.M. Smart Inverters for Utility and Industry Applications. In Proceedings of the PCIM Europe 2015; International Exhibition and Conference for Power Electronics, Intelligent Motion, Renewable Energy and Energy Management, Nuremberg, Germany, 19–21 May 2015; pp. 1–8.
16. Bragard, M.; Soltau, N.; Thomas, S.; De Doncker, R.W. The balance of renewable sources and user demands in grids: Power electronics for modular battery energy storage systems. *IEEE Trans. Power Electron.* **2010**, *25*, 3049–3056. [CrossRef]
17. Teleke, S.; Baran, M.E.; Bhattacharya, S.; Huang, A.Q. Rule-based control of battery energy storage for dispatching intermittent renewable sources. *IEEE Trans. Sustain. Energy* **2010**, *1*, 117–124. [CrossRef]
18. Ceja-Espinosa, C.; Espinosa-Juárez, E. Smoothing of photovoltaic power generation using batteries as energy storage. In Proceedings of the 2017 IEEE PES—Innovative Smart Grid Technologies Conference-Latin America (ISGT Latin America), Quito, Ecuador, 20–22 September 2017; pp. 1–6.
19. Lujano-Rojas, J.M.; Dufo-López, R.; Bernal-Agustín, J.L.; Catalão, J.P. Optimizing daily operation of battery energy storage systems under real-time pricing schemes. *IEEE Trans. Smart Grid* **2016**, *8*, 316–330. [CrossRef]
20. Hernández, J.; Sanchez-Sutil, F.; Muñoz-Rodríguez, F. Design criteria for the optimal sizing of a hybrid energy storage system in PV household-prosumers to maximize self-consumption and self-sufficiency. *Energy* **2019**, *186*, 115827. [CrossRef]

21. Gomez-Gonzalez, M.; Hernandez, J.; Vera, D.; Jurado, F. Optimal sizing and power schedule in PV household-prosumers for improving PV self-consumption and providing frequency containment reserve. *Energy* **2020**, *191*, 116554. [CrossRef]
22. Alam, M.; Muttaqi, K.; Sutanto, D. A novel approach for ramp-rate control of solar PV using energy storage to mitigate output fluctuations caused by cloud passing. *IEEE Trans. Energy Convers.* **2014**, *29*, 507–518.
23. Sangwongwanich, A.; Yang, Y.; Blaabjerg, F. A cost-effective power ramp-rate control strategy for single-phase two-stage grid-connected photovoltaic systems. In Proceedings of the Energy Conversion Congress and Exposition (ECCE), Milwaukee, WI, USA, 18–22 September 2016; pp. 1–7.
24. Li, X.; Hui, D.; Lai, X. Battery energy storage station (BESS)-based smoothing control of photovoltaic (PV) and wind power generation fluctuations. *IEEE Trans. Sustain. Energy* **2013**, *4*, 464–473. [CrossRef]
25. Hernández, J.C.; Bueno, P.G.; Sanchez-Sutil, F. Enhanced utility-scale photovoltaic units with frequency support functions and dynamic grid support for transmission systems. *IET Renew. Power Gener.* **2017**, *11*, 361–372. [CrossRef]
26. Kim, N.; Parkhideh, B. Control and Operating Range Analysis of AC-Stacked PV Inverter Architecture Integrated with Battery. *IEEE Trans. Power Electron.* **2018**, *33*, 10032–10037. [CrossRef]
27. Tran, V.T.; Islam, M.R.; Sutanto, D.; Muttaqi, K.M. Mitigation of Solar PV Intermittency Using Ramp-Rate Control of Energy Buffer Unit. *IEEE Trans. Energy Convers.* **2018**, *34*, 435–445. [CrossRef]
28. Saxena, N.; Hussain, I.; Singh, B.; Vyas, A.L. Implementation of a Grid-Integrated PV-Battery System for Residential and Electrical Vehicle Applications. *IEEE Trans. Ind. Electron.* **2018**, *65*, 6592–6601. [CrossRef]
29. Zhang, Q.; Sun, K. A Flexible Power Control for PV-Battery-Hybrid System Using Cascaded H-Bridge Converters. *IEEE J. Emerg. Sel. Top. Power Electron.* **2018**, *7*, 2184–2195. [CrossRef]
30. Rallabandi, V.; Akeyo, O.M.; Jewell, N.; Ionel, D.M. Incorporating Battery Energy Storage Systems Into Multi-MW Grid Connected PV Systems. *IEEE Trans. Ind. Appl.* **2019**, *55*, 638–647. [CrossRef]
31. Yoder, M.; Andreas, A. Lowry Range Solar Station: Arapahoe County, Colorado (Data). Available online: https://data.nrel.gov/submissions/30 (accessed on 8 April 2019).
32. Lew, D.; Miller, N. Reaching new solar heights: integrating high penetrations of PV into the power system. *IET Renew. Power Gener.* **2017**, *11*, 20–26, doi:10.1049/iet-rpg.2016.0264. [CrossRef]
33. California ISO. Renewables and Emission Reports. Available online: http://www.caiso.com/market/Pages/ReportsBulletins/RenewablesReporting.aspx (accessed on 8 April 2019).
34. Karimi-Ghartemani, M.; Khajehoddin, S.A.; Jain, P.; Bakhshai, A. Linear quadratic output tracking and disturbance rejection. *Int. J. Control* **2011**, *84*, 1442–1449. [CrossRef]
35. De Brito, M.A.G.; Galotto, L.; Sampaio, L.P.; e Melo, G.d.A.; Canesin, C.A. Evaluation of the main MPPT techniques for photovoltaic applications. *IEEE Trans. Ind. Electron.* **2013**, *60*, 1156–1167. [CrossRef]
36. Kazmierkowski, M.P.; Malesani, L. Current control techniques for three-phase voltage-source PWM converters: A survey. *IEEE Trans. Ind. Electron.* **1998**, *45*, 691–703. [CrossRef]
37. Blaabjerg, F.; Teodorescu, R.; Liserre, M.; Timbus, A.V. Overview of Control and Grid Synchronization for Distributed Power Generation Systems. *IEEE Trans. Ind. Electron.* **2006**, *53*, 1398–1409, doi:10.1109/TIE.2006.881997. [CrossRef]
38. Silwal, S.; Karimi-Ghartemani, M.; Sharma, R.; Karimi, H. Impact of Feed-forward and Decoupling Terms on Stability of Grid-Connected Inverters. In Proceedings of the 2019 IEEE 28th International Symposium on Industrial Electronics (ISIE), Vancouver, BC, Canada, 12–14 June 2019; pp. 2641–2646, doi:10.1109/ISIE.2019.8781454. [CrossRef]
39. Silwal, S.; Taghizadeh, S.; Karimi Ghartemani, M.; Hossain, J.; Davari, M. An Enhanced Control System for Single-Phase Inverters Interfaced with Weak and Distorted Grids. *IEEE Trans. Power Electron.* **2019**, *34*, 12538–12551, doi:10.1109/TPEL.2019.2909532. [CrossRef]